CHANGE OF INERTIA TENSOR DUE TO A SEVERED RADIAL BOOM FOR SPINNING SPACECRAFT

Joseph E. Sedlak[*] and Babak Vint[†]

Many spinning spacecraft have long, flexible, radial booms to carry science instrumentation. These radial booms often have low mass but contribute significantly to the spacecraft moment of inertia due to their length. There are historical cases where radial booms have been severed or have failed to deploy. This paper presents models for the center of mass (CM) and inertia tensor that account for variable boom geometry and investigates how the CM and inertia tensor change when a radial boom is severed.

The CM and inertia tensor models presented here will be included in the Attitude Ground System (AGS) for the Magnetospheric Multiscale (MMS) mission. This work prepares the AGS to provide uninterrupted support in the event of a radial boom anomaly. These models will improve the AGS computations for spin-axis precession prediction, Kalman filter propagation for the definitive attitude, and mass property generation needed for the onboard control system. As an additional application, a method is developed for approximating the location on the boom where the break occurred based on the new models and readily observable attitude parameters.

INTRODUCTION

The spin-stabilized spacecraft is a convenient platform for the measurement of magnetic and electric fields, plasma properties, and other physical phenomena best observed over a wide baseline. Many spinning spacecraft have radial booms that are constructed from very thin and flexible multi-stranded wire. These radial booms can be quite long, with examples ranging from 25 to 250 m, and are kept under tension by centrifugal force. This design allows the science instrumentation to span a distance that is large in relation to the size of the spacecraft body. However, micrometeoroid or debris impacts and deployment problems are inherent risks. As the contribution to the mass moment of inertia increases with the square of distance, radial boom anomalies can significantly alter the dynamics of the spacecraft despite having low mass. For torques to be balanced at equilibrium, flexible members tend toward orientations that are perpendicular to and radiate outward from the spin axis. Likewise, the spin axis is dependent on the mass distribution of the spacecraft, and therefore on the orientation of each member. This paper presents models for the center of mass (CM) and inertia tensor that account for this mutual dependency of spin axis and radial boom orientation.

Radial boom anomalies are not unknown in the history of spin-stabilized spacecraft. In 1996, a wire boom on the Fast Auroral SnapshoT (FAST) satellite failed to deploy shortly after launch, causing a large coning angle for the duration of the mission. (Coning is defined to be the angle between the nominal body spin axis and the spacecraft major principal axis of inertia [MPA].) Despite this problem, the mission went on to become a success; complete electric field

---

[*] Consulting Systems Engineer, a.i. solutions, Inc., 4500 Forbes Blvd., Lanham, MD, USA 20706.
[†] Systems Engineer, a.i. solutions, Inc., 4500 Forbes Blvd., Lanham, MD, USA 20706.

measurements were still possible using the remaining three radial booms and two axial booms.[1] The IMAGE spacecraft, launched in March 2000, had multiple radial boom breaks: −X antenna damage in October 2000, +Y antenna damage in September 2001, and further +Y antenna damage in September 2004.[2] The more recent ARTEMIS mission consists of two of the five spacecraft from the THEMIS constellation that were moved to lunar orbits starting in 2010. In October 2010, ARTEMIS P1 (formerly THEMIS B) lost part of one wire boom, including the spherical probe attached to its end.[3] One additional relevant example of a probable micrometeoroid impact is given by the DODGE spacecraft, which was not a spinner. This was a Department of Defense satellite, launched in July 1967. This mission was designed to test gravity-gradient stabilization and included ten retractable booms. In November 1967, DODGE abruptly changed from a gravity-gradient stable attitude to a tumbling mode. This event occurred during an intense Leonid meteor shower, so impact was the probable cause.[4] Thanks to the efforts of the respective engineering teams, all these spacecraft were able to carry out their missions and now serve as useful case studies for current and future missions.

The models and techniques presented here will be included in the Attitude Ground System (AGS) for the Magnetospheric Multiscale (MMS) mission.[5] The AGS provides flight dynamics attitude ground support services in the control center at the NASA Goddard Space Flight Center (GSFC). Increasing the accuracy of CM and inertia tensor values benefits three major aspects of MMS mission support: the predictions of spin axis precession (needed for ground contact planning), the propagation step in the attitude Kalman filter[6] (used to generate definitive attitudes for the science teams), and the CM and inertia products uplinked to the MMS spacecraft (used for onboard attitude and orbit control). The benefits from the new models will be most significant in the event of a boom anomaly, but they will also provide some marginal improvement even for nominal flight operations activities with unbroken booms.

One fundamental assumption made in developing these models is that nutation and boom vibrations are fully damped. This assumption implies three things: the axis of rotation passes through the CM, the MPA is coincident with the axis of rotation, and all wire booms are oriented radially to the axis of rotation. If any of these conditions were not true, there would be unbalanced torques and/or forces driving internal motion of the spacecraft components. Whenever there is internal motion, friction will damp it out in time. For the MMS spacecraft, it is known that boom vibrations dampen to half-amplitude in roughly 12 hours.[7] After a disturbance such as a break in one of the booms, the rigid central body of the spacecraft is likely to settle into a new orientation to balance the torques and forces. With this rebalancing, the MPA will almost never coincide exactly with the spacecraft nominal spin axis (for most spinners, the body Z-axis). Therefore, the spacecraft body will be tilted relative to the spin plane.

The main goal of this paper is to develop a method that considers the "fraction remaining" for each boom and solves for the CM and inertia tensor while respecting the mutual dependence of spin axis and boom directions. (The fraction remaining for each radial boom is referred to below as the boom fraction, f_b.) To begin, a spin vector is assumed and its direction is varied via an iterative method until it is coincident with the MPA of the inertia tensor resulting from that geometry. For each spin vector evaluated, the orientations of the booms, and in turn the inertia tensor of the spacecraft, depend upon it. Consequently, each time a spin vector is evaluated, solutions for the CM and boom directions consistent with that spin vector must be found. A separate iterative method is implemented to solve for these parameters. That is, for each step of the "outer iteration," which solves for consistent spin axis direction and MPA, a nested "inner iteration" solves for the boom geometry. Once the spin axis direction converges to be consistent with the resultant MPA, and all other parameters are consistent, this outer iterative solution will yield a mapping between boom fraction and MPA direction. It is possible to determine the location where a boom

was severed using this mapping if the MPA is measurable on orbit. As an example, the MMS spacecraft includes star cameras that allow for accurate attitude estimation. By taking appropriate spin-averages, the MPA can be estimated.[5] The observed change in MPA due to a boom break can be compared to the prediction from the inertia tensor model given here to determine the approximate location where the break occurred.

The organization of the paper is as follows. After this introduction, there is a description of the spacecraft model, which gives an overview of the coordinate frame and the parts of the spacecraft hardware relevant to describing the CM and inertia tensor models. Next, there is a derivation of the inner iteration method for solving for the CM and the radial boom directions. An error analysis of this method shows that conditions are easily met to guarantee convergence. The next two sections present the inertia tensor model and the outer iteration method, which solves for consistent values for the spin axis and the MPA. A numerical acceleration method for the outer iteration is used to reduce the number of iterations required for convergence. Those sections are followed by an analysis showing how to estimate the location where a boom was severed and the uncertainty in that estimate. The paper ends with conclusions and a brief discussion of future work.

SPACECRAFT MODEL

The MMS mission is a convenient testbed for the ideas presented here.[8] This mission comprises four nearly-identical spinning spacecraft flying in formation. Each MMS spacecraft has two Axial Double Probe (ADP) booms, which lie along the nominal axis of rotation ($\pm Z$-axis), and four Spin-plane Double Probe (SDP) wire booms, which extend radially outward from the spacecraft body.[9]
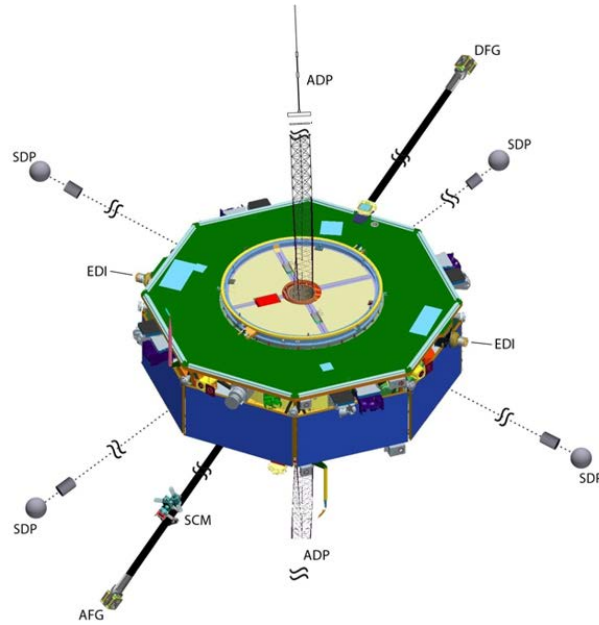

Figure 1. MMS Spacecraft Showing Multiple Booms.
(Figure used with permission of University of New Hampshire MMS-FIELDS team.)

Figure 1 shows the layout of the MMS booms. There also are two radial magnetometer booms, which are much shorter and more rigid compared to the SDPs. Within the spacecraft body, there are four fuel tanks with diaphragms that are supported by helium gas to pressurize the fuel and suppress slosh. Among the variables in the CM and inertia tensor models are the amount of fuel remaining, which is known from maneuver bookkeeping and other methods (e.g., ideal gas law and

heat capacitance methods), and the shapes of the diaphragms and the distribution of fuel in the four tanks, which are not directly observable. The prelaunch inertia model assumes the fuel is symmetrically distributed about the nominal spin axis.
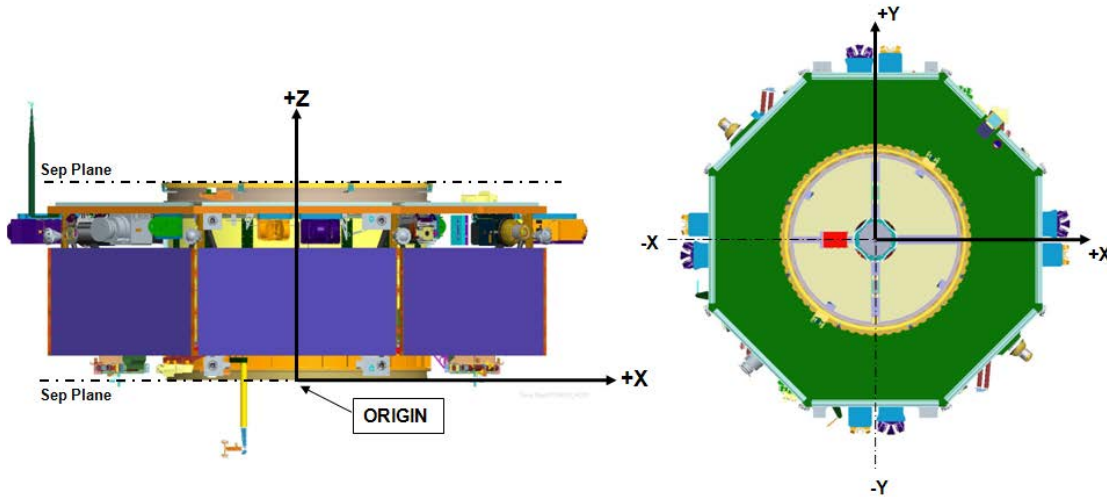

Figure 2. MMS Observatory Coordinate System (OCS).

The Observatory Coordinate System (OCS) is a body-fixed frame defined for the MMS mission and is the primary coordinate system referenced in this paper.[10] The origin of the OCS is at the center of the lower spacecraft deck. (When the four MMS spacecraft were stacked for launch, this location was defined as the "center of the launch vehicle adaptor ring on the separation interface plane.") Figure 2 shows the orientation of the X_{OCS}, Y_{OCS}, and Z_{OCS} axes and the location of the origin.[11] By definition, the OCS Z-axis extends through the spacecraft structure along the center line of the thrust tube. The X-axis intersects the plane of Instrument Bay 1, and the Y-axis completes the right-handed orthogonal triad.

The nominal MMS spin axis is along the OCS Z-axis. It is important to keep in mind that the actual spin axis is never perfectly coincident with the nominal spin axis since the true CM may be offset from Z_{OCS} and there may be some coning, where the MPA is tilted with respect to Z_{OCS}. This is one of the elements accounted for in the models presented in this work.

The CM and inertia tensor models given below divide the spacecraft into a central rigid body and four attached rigid bodies representing the radial SDP booms. The fuel slosh is well-damped by the diaphragms, and since the magnetometer and ADP booms are quite stiff compared to the wire SDP booms, these are all modeled as part of the rigid central body. Since vibrational modes for the body damp out faster, are higher in frequency, and are well-separated from the SDP boom modes, treating the spacecraft central body as rigid is valid for this study.

The CM of an individual SDP wire boom depends on the instruments mounted on that boom and the location where it has been severed. The booms on the four MMS spacecraft include, in order from the attachment point to the boom tip: a multi-stranded wire of length 57 m, a pre-amplifier, a thinner wire of length 1.75 m, and a sensor sphere of diameter 0.08 m and mass 0.091 kg. The preamplifier is modeled as a cylinder of length 0.071 m and radius 0.0155 m with a mass of 0.086 kg. The main wire linear density is 0.00506 kg/m, and the thin wire linear density is 0.000155 kg/m. If a break in the SDP boom should occur, it is likely that the sensor sphere and possibly the preamplifier would be lost. The boom attachment points are given in Eq. (6) in the next section.
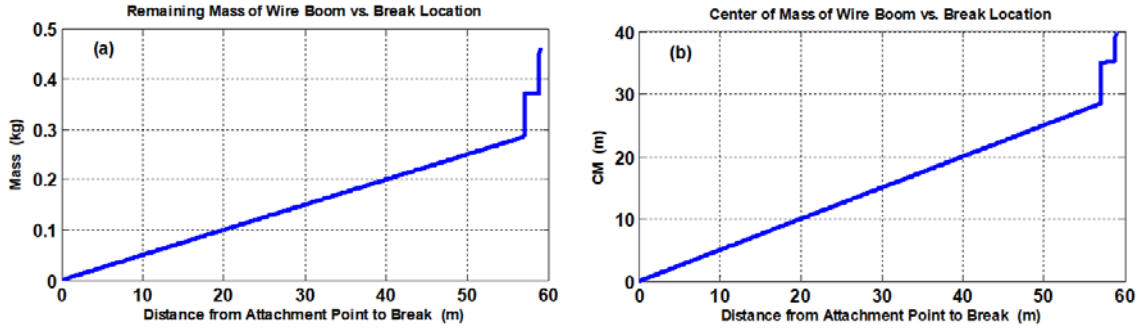
Figure 3. (a) Remaining boom mass, and (b) boom CM measured from the attachment point versus location where the boom was severed.

Figure 3a shows the boom mass, and Figure 3b shows the boom CM location. These plots display how the mass and CM vary with the location of a break, measured outwards from the boom attachment point. The CM plot is linear, with a slope of one-half, up to the location of the preamplifier; this just reflects the CM of a straight rod being at the midpoint of that rod. The plots show that the change in boom mass and CM are effectively discontinuous at the preamplifier and detector sphere locations. However, for convenience, the mass and CM are modeled as continuous functions, treating the bodies of the instrument hardware as uniform density objects.

SOLUTION FOR CONSISTENT SPACECRAFT CM AND BOOM VECTORS

This section describes a solution for the spacecraft CM and the directions of the radial wire booms. The boom directions are needed to compute the position of the total spacecraft CM. The CM position is needed to know the boom directions since the booms are radial to the spin axis, which must pass through the CM. Thus, the problem lends itself to solution by iteration, alternating between the CM and the boom directions. This is the "inner iteration" described in the introduction.

The spin axis will lie along the MPA when spacecraft vibrations are fully damped. However, the inertia tensor and its MPA are not known prior to solving for the CM and boom vectors. This means the spin axis is not yet known, but the spin axis is needed to solve for the CM and boom vectors. One resolution to this quandary is simply to assume a temporary direction about which the spacecraft is forced to spin. This "forced spin axis" will not be the final spin axis, as it does not yet coincide with the MPA. The iteration method described in this section is only an intermediate step in the solution of the overall problem. This step will yield consistent CM and boom vectors for any assumed spin vector. This solution then will be used in the inertia tensor model, which is needed to find the MPA direction, as discussed in the section describing the Outer Iteration Algorithm.
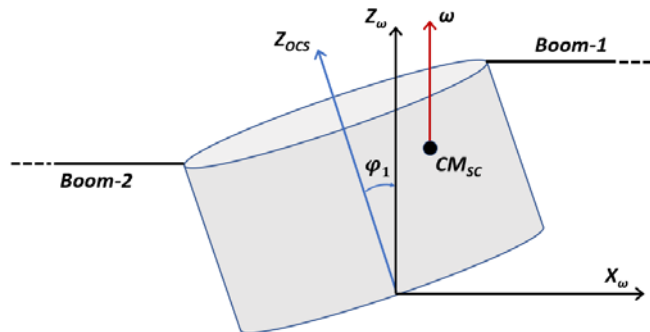

Figure 4. Sketch of Spacecraft Central Body and Two of the Four Radial Wire Booms.

5

Figure 4 shows the spin axis, $\vec{\omega}$, tilted by an angle, φ_1, from the Z_{OCS} axis, and passing through the spacecraft CM. The φ_1 angle is a rotation in the plane defined by Z_{OCS} and the severed boom attachment point (boom #1 is taken to be the severed boom in this figure). The spin direction is arbitrary for this inner iteration algorithm, so it can also have a tilt, φ_2, out of this plane. The φ_2 angle is not shown in Figure 4, but it is accounted for in the models presented in this paper.

Looking ahead to the solution of the outer iteration for the spin axis consistent with the inertia tensor and MPA, it will be shown that for that solution the angle φ_2 is generally smaller than φ_1 as long as only one boom is broken (e.g., see Table 1 in the second to last section of this paper). The magnitude of φ_2 may be comparable to the initial coning angle prior to any boom break; that is, even without a severed boom, asymmetry in the fuel distribution causes some coning, leading to computed values of φ_1 and φ_2 differing slightly from zero. The coning angles on the four MMS observatories currently range from 0.02 to 0.2 deg, and the spacecraft central body CMs are offset from the Z_{OCS} axis by 4 to 8 millimeters.

Inner Iteration Algorithm

In the first step of the inner iteration, the spacecraft CM is given as a function of the boom vectors and other system parameters, including the boom fractions, fuel tank fill-fraction, and the spin direction, $\hat{\omega}$, where the caret indicates unit vector. Note that the boom fractions indicate the remaining portion for each of the four booms. The algorithm given here converges for any combination of break locations on multiple booms.

For the second step, the boom vectors are given as functions of the CM position and $\hat{\omega}$. When these two functions, that is, the computations of CM and boom vectors, are iterated, their values quickly converge. This process yields consistent values for the CM and the boom vectors for any choice of boom fractions and spin axis direction. Alternatively, approximate closed-form solutions can be derived under the assumption of small angle deviations of the booms from their nominal directions. These closed-form approximations were used as a first test of the iteration method, but they are not presented here.

In general, the CM of a body is

$$\vec{C} = \frac{1}{M_A}\sum_{i \in \mathcal{A}} M_i \vec{r}_i \, , \tag{1}$$

where $\mathcal{A}$ is the finite set of all mass particles in the body, M_i and $\vec{r}_i$ are the masses and positions of those particles, and $M_A = \sum_{i \in \mathcal{A}} M_i$ is the total mass. This expression can be written as

$$\vec{C} = \frac{1}{M_A}\left[\sum_{j \in \mathcal{B}} M_j \vec{r}_j + \sum_{k \in \mathcal{C}} M_k \vec{r}_k + \cdots\right] \, , \tag{2}$$

where the set of all particles has been separated into the union of an arbitrary number of disjoint subsets, $\mathcal{A} = \mathcal{B} \cup \mathcal{C} \cup \cdots$. Next, Eq. (2) can be written

$$\vec{C} = \frac{1}{M_A}\left[M_B \frac{\sum_{j \in \mathcal{B}} M_j \vec{r}_j}{M_B} + M_C \frac{\sum_{k \in \mathcal{C}} M_k \vec{r}_k}{M_C} + \cdots\right] = \frac{1}{M_A}\left[M_B \vec{C}_B + M_C \vec{C}_C + \cdots\right] \, , \tag{3}$$

where $M_B = \sum_{j \in \mathcal{B}} M_j$ and $\vec{C}_B$ is the CM of the particles in set $\mathcal{B}$, and similarly for set $\mathcal{C}$, etc. This shows a rigid body can be divided into arbitrary separate parts, and the CM of the entire system will be the first moment of the masses of these parts located at their respective CMs, divided by the total mass. A similar argument allows one to compute the inertia tensor for a body by subdividing it into arbitrary parts. The inertia tensors for the individual parts can be computed and combined to obtain the whole. However, care must be taken to use consistent coordinate frames and to account for the offset of the CMs of the parts, as discussed in the Inertia Tensor section below.

Using Eq. (3), one can write the spacecraft CM, denoted $\vec{C}_{SC}$, as

$$\vec{C}_{SC} = \frac{1}{M_{tot}}\left[m_{body}\vec{C}_{body} + \sum_{i=1,4} m_i\vec{s}_i\right],$$ (4)

where m_{body} is the mass and $\vec{C}_{body}$ is the CM of the spacecraft central body, and M_{tot} is the total spacecraft mass. The m_i in Eq. (4) are the wire boom masses, with index i running from 1 to 4. The vectors to the boom CMs, $\vec{s}_i$, are obtained as the sums of vectors from the origin of the OCS frame to the boom attachment points, $\vec{A}_i$, plus vectors along the booms. The distances from the attachments to the boom CMs are d_i, and the unit vectors along the booms are written $\hat{b}_i$. Hence, the boom CM vectors are

$$\vec{s}_i = \vec{A}_i + d_i\hat{b}_i,$$ (5)

for i = 1 to 4. The values for m_i and d_i are given in Figures 3a and 3b. The boom attachment points in the OCS frame are

$$\vec{A}_1 = Z_{30}\begin{bmatrix} R \\ 0 \\ H \end{bmatrix}, \quad \vec{A}_2 = Z_{30}\begin{bmatrix} -R \\ 0 \\ H \end{bmatrix}, \quad \vec{A}_3 = Z_{30}\begin{bmatrix} 0 \\ R \\ H \end{bmatrix}, \quad \vec{A}_4 = Z_{30}\begin{bmatrix} 0 \\ -R \\ H \end{bmatrix},$$ (6a-d)

where H = 1.051 m is the height and R = 1.597 m is the radial distance from the OCS origin to the attachment points, and $Z_{30} \equiv M_z(-30\ deg)$ is the Z-axis rotation matrix, where

$$M_z(\theta) = \begin{bmatrix} \cos\theta & \sin\theta & 0 \\ -\sin\theta & \cos\theta & 0 \\ 0 & 0 & 1 \end{bmatrix},$$ (7)

which is needed since the attachment points are rotated by 30 deg from the OCS X- and Y-axes.

Next, the boom vectors are written as functions of the spacecraft CM. Define the vectors from the spacecraft CM to each boom attachment point

$$\vec{D}_i \equiv \vec{A}_i - \vec{C}_{SC}, \quad (i = 1,4).$$ (8)

As shown in Figure 4, the spin axis passes through the CM. The boom vectors pass through their attachment points, and if extended, must intersect the spin axis and be perpendicular to it. Thus, the boom directions can be obtained by projecting the vectors in Eq. (8) onto the spin plane, that is, the plane perpendicular to the spin axis, $\hat{\omega}$. Normalizing those results yields the unit boom vectors,

$$\hat{b}_i = \mathcal{P}\vec{D}_i/|\mathcal{P}\vec{D}_i|, \quad (i = 1,4).$$ (9)

The projection operator, $\mathcal{P}$, onto the spin plane is

$$\mathcal{P} \equiv I_3 - \hat{\omega}\hat{\omega}^T,$$ (10)

where I_3 is the 3×3 identity matrix.

The iteration now can proceed by first computing the boom vectors using Eq. (9) with the central body CM, $\vec{C}_{body}$, as an initial guess for the total spacecraft CM in Eq. (8). Then, Eq. (4) is used to compute a new value for the spacecraft CM. These steps are repeated until the changes in these values are less than a convergence tolerance.

For the MMS spacecraft, the iteration process converges to machine double precision in 9-10 iterations. Six iterations will yield precisions of milli-arcseconds for the boom directions and nanometers for the CM position.

Proof of Convergence for Iteration Method for CM and Boom Vectors

This subsection presents approximate values for the errors in the CM and boom vectors at each step of the inner iteration process. The error in the CM can be expressed as the gradient of Eq. (4) with respect to the vectors, $\hat{b}_i$, times the errors in those vectors. This yields

$$\Delta \vec{C}_{SC} \approx \frac{1}{M_{tot}} \sum_{i=1,4} m_i d_i \Delta \hat{b}_i \, , \tag{11}$$

where the error in a variable is indicated by the Δ symbol.

Similarly, the errors in $\hat{b}_i$ can be written as the gradient of Eq. (9) with respect to the spacecraft CM, times the error in the CM. After some algebra, this results in

$$\Delta \hat{b}_i \approx \frac{-1}{|\mathcal{P}\vec{D}_i|} \left(\mathcal{P} - \hat{b}_i \hat{b}_i^T \right) \Delta \vec{C}_{SC} \, , \quad (i = 1,4) \, . \tag{12}$$

Suppose Eq. (12) gives the N-th iteration for the boom vector errors. Then, by combining Eqs. (11) and (12), one obtains the CM error for the $N + 1^{st}$ iteration,

$$\Delta \vec{C}_{SC}^{(N+1)} \approx \frac{-1}{M_{tot}} \sum_{i=1,4} \frac{1}{|\mathcal{P}\vec{D}_i|} m_i d_i \left(\mathcal{P} - \hat{b}_i \hat{b}_i^T \right) \Delta \vec{C}_{SC}^{(N)} \, . \tag{13}$$

The following arguments can be made to establish approximate values for the factors in Eq. (13). First, the spin axis is expected always to be close to the Z-axis in the OCS frame. Even with a completely severed boom, the change in coning angle is found to be less than 2 deg, and the CM remains within a few centimeters of the Z-axis. This means the value of $|\mathcal{P}\vec{D}_i|$ will be approximately equal to the radial distance, R, of the boom attachment points for all four booms. Second, if one rotates about the Z-axis to a frame where booms 1 and 2 are nominally along the $\pm X$-axis, and booms 3 and 4 are nominally along the $\pm Y$-axis, then

$$\mathcal{P} - \hat{b}_i \hat{b}_i^T = I_3 - \hat{\omega}\hat{\omega}^T - \hat{b}_i \hat{b}_i^T \approx \begin{bmatrix} 0 & 0 & 0 \\ 0 & 1 & 0 \\ 0 & 0 & 0 \end{bmatrix}, \quad (i = 1,2) \, , \tag{14a}$$

and

$$\mathcal{P} - \hat{b}_i \hat{b}_i^T = I_3 - \hat{\omega}\hat{\omega}^T - \hat{b}_i \hat{b}_i^T \approx \begin{bmatrix} 1 & 0 & 0 \\ 0 & 0 & 0 \\ 0 & 0 & 0 \end{bmatrix}, \quad (i = 3,4) \, , \tag{14b}$$

where the spin axis again is assumed to be near the Z-axis.

Combining Eqs. (13) and (14) yields the errors for the X- and Y-components of the CM,

$$\Delta C_{SC,X}^{(N+1)} \approx \frac{-1}{M_{tot}R} (m_3 d_3 + m_4 d_4) \Delta C_{SC,X}^{(N)} \, , \tag{15a}$$

and

$$\Delta C_{SC,Y}^{(N+1)} \approx \frac{-1}{M_{tot}R} (m_1 d_1 + m_2 d_2) \Delta C_{SC,Y}^{(N)} \, . \tag{15b}$$

In the approximations used in this error analysis, the Z-component of the CM error is unaffected by the iteration process. A break in one of the booms will cause $C_{SC,Z}$ to shift in the negative Z-direction due to the mass loss, but that shift will be captured in the first iteration. In subsequent iterations, the corrections to the boom vectors remain perpendicular to the spin axis; thus, $\Delta C_{SC,Z}$ will be near zero.

The coefficients of the errors in Eqs. (15) are always less than or equal to the values obtained using unbroken booms. Let m_0 and d_0 be the mass and boom CM distance for unbroken booms. Equations (15) imply that the error in $\vec{C}_{SC}$ on the N-th iteration is bounded,

$$\left|\Delta\vec{C}_{SC}^{(N)}\right| < \left(\frac{2^{3/2}m_0 d_0}{M_{tot}R}\right)^N \left|\Delta\vec{C}_{SC}^{(0)}\right|. \tag{16}$$

Convergence of the iterative method is guaranteed if the quantity in parentheses in Eq. (16) is less than unity. For the MMS spacecraft, this expression has a value of approximately 0.03. In addition, since the error in the initial guess, $\Delta\vec{C}_{SC}^{(0)}$, is certainly less than the spacecraft radius R (where $R \approx 1.6$ m), Eq. (16) yields error estimates in good agreement with the numerical convergence results quoted at the end of the previous subsection after Eq. (10).

INERTIA TENSOR

The current method used by the MMS AGS for calculating the inertia tensor is based on a lookup table along with an analytic model for the radial boom deployment. The lookup table was generated prelaunch by the MMS mechanical engineers and contains the mass properties (CM and inertia tensor) for various stages of boom deployment and fuel fill-fractions. This method assumes all booms are undamaged, point in nominal directions, and are symmetrically deployed in opposing pairs. For the work presented here, it was desired to improve the model to account for booms that are partly severed and boom directions that vary as the mass distribution of the spacecraft changes (with or without any damage to the booms). This improvement will increase the accuracy of attitude estimation in general, facilitate ground support in the case of damaged radial booms, and provide the means for estimating a boom break location.

The MMS engineers determined the mass properties of the spacecraft prior to launch. These tabulated properties, along with a simple fuel consumption model, yield the inertia tensor model used from launch until now. The AGS analysts also perform frequent calibrations to determine corrections to the MPA direction to account for any asymmetry in the fuel distribution,[5,7] but these corrections are not included in this paper. Other than these MPA calibrations, the mass properties of the central body itself would not be affected by damage to the radial booms. The contribution of the radial booms to the spacecraft mass properties, however, can be improved by modeling angling or breakage of the radial booms. This only works if the boom geometry is known. While boom directions are not directly observable, they can be determined iteratively, as shown in the previous section.

In the improved inertia tensor model, the spacecraft central body and the four radial booms are each taken to be rigid components of the system. The wire booms are flexible, of course, but their rigid-body inertias are needed for computing the MPA for fully-damped rotation and for very low-frequency perturbations, e.g., the spin axis precession from gravity-gradient torques. Since each boom comprises several parts, the parallel axis theorem is used to build each boom inertia tensor from these parts. The model then uses the parallel axis theorem once more to build the total spacecraft inertia tensor from the inertia tensors of the body and four booms.

The values for the mass and CM of an individual boom were given earlier in Figure 3 in the section on the Spacecraft Model. To obtain the boom inertia tensor, the inertias of the boom parts can be combined in a convenient frame and then transformed to the OCS. Since each boom exhibits axial symmetry about its length, a convenient coordinate system for calculating mass moments of inertia orients one axis along the boom direction and the other two axes in any mutually orthogonal directions. Here, the *X*-axis is chosen to lie along the length of the boom, and the origin is chosen

to be the attachment point of the boom to the body. Let this frame be named the Boom Direction Coordinate System (BDCS).

Due to the rotational symmetry about the BDCS X-axis, one has $J_{YY} = J_{ZZ}$ for all boom parts, with all products of inertia zero, and arbitrary choices for the BDCS Y- and Z-axes. A simple choice for the BDCS is to define a sequence of two rotations on the OCS: the first rotation is about the Z-axis by an angle θ_1 that aligns the BDCS X-axis with the OCS XY-projection of the boom direction, and the second rotation is about the Y-axis by an angle θ_2 to complete the alignment of the X-axis parallel with the boom direction. Therefore, for a given boom direction, $\hat{b}$, the corresponding BDCS is defined by the following passive transformation from OCS to BDCS,

$$\theta_1 = \tan^{-1}\left(\frac{b_Y}{b_X}\right) , \tag{17}$$

$$\theta_2 = \tan^{-1}\left(\frac{-b_Z}{\left(b_X^2 + b_Y^2\right)^{1/2}}\right) , \tag{18}$$

$$A_{BDCS \leftarrow OCS} = \begin{bmatrix} \cos\theta_2 & 0 & -\sin\theta_2 \\ 0 & 1 & 0 \\ \sin\theta_2 & 0 & \cos\theta_2 \end{bmatrix} \begin{bmatrix} \cos\theta_1 & \sin\theta_1 & 0 \\ -\sin\theta_1 & \cos\theta_1 & 0 \\ 0 & 0 & 1 \end{bmatrix} . \tag{19}$$

Note that Eq. (17) is implemented using the *atan2* function so the signs and the quadrant are accounted for properly. The transformation from BDCS to OCS is obtained as the transpose of Eq. (19) since the inverse is the transpose for orthogonal matrices. The resulting matrix is applied as a similarity transformation (since the inertia tensor is bilinear in the mass coordinates) to express the BDCS boom inertia tensor in the OCS,

$$A = A_{BDCS \leftarrow OCS}^T , \tag{20}$$

$$J_{OCS} = A J_{BDCS} A^T . \tag{21}$$

The parallel axis theorem is used multiple times to build the inertia tensor of each boom from its parts, and to build the inertia tensor of the system from the five rigid bodies. In both cases, one follows the same procedure to combine several inertia tensors into one. First, determine the system center of mass based on the masses and CMs of its constituents. Next, determine the inertia tensor of each constituent about its CM. Apply the parallel axis theorem to translate the inertia tensor of each constituent from its own CM to the system CM. At this point, the inertia tensors of all the constituents are referenced to the same point in space. The final step is simply to sum these inertia tensors to form the combined inertia tensor of the system. For a single boom, the inertia tensors of the boom parts are combined. For the spacecraft, the inertia tensors of the five rigid-body components are combined.

To translate a rigid body's inertia tensor about its CM to an arbitrary point P, define a displacement vector $\vec{r}$ pointing between the CM and P, and use the parallel axis theorem,

$$J_P = J_{CM} + m(r^2 I_3 - \vec{r}\vec{r}^T) , \tag{22}$$

where r is the magnitude of $\vec{r}$, and I_3 is the 3×3 identity matrix. Note that since Eq. (22) is quadratic in $\vec{r}$, it does not matter whether $\vec{r}$ points from P to the CM or from the CM to P.

As described in the Spacecraft Model section, the parts composing the boom (in order from attachment to tip) are: the main boom wire, a preamplifier, a thin wire, and a spherical sensor. To calculate the inertia tensors of these parts, both wires are modeled as thin rods, the preamplifier as a cylinder, and the probe as a sphere, each having uniform density. Expressions for the axial and transverse mass moments of inertia about the CM, J_a and J_t, respectively, are well-known for these

solids. Since the BDCS X-axis is the symmetry axis, the inertia tensor for each part about its own CM can be written

$$J_{part} = \begin{bmatrix} J_a & 0 & 0 \\ 0 & J_t & 0 \\ 0 & 0 & J_t \end{bmatrix}. \tag{23}$$

Denote the mass of each part of the boom as m_{part} and the location of its CM along the length of the boom as c_{part}. By definition, the position of c_{part} lies exactly along the BDCS X-axis. Application of the parallel axis theorem to translate the part's inertia tensor from its CM to the boom CM yields

$$J_{CM,part} = J_{part} + m_{part} \begin{bmatrix} 0 & 0 & 0 \\ 0 & x^2 & 0 \\ 0 & 0 & x^2 \end{bmatrix}, \tag{24}$$

where

$$x \equiv d_i - c_{part}, \tag{25}$$

and where d_i is the distance along the boom to the boom CM. The result in Eq. (24) indicates the inertia tensor of the individual part about the boom's CM. Once $J_{CM,part}$ is determined for every part, the sum of these tensors yields the total inertia tensor of the boom about the boom's CM in the BDCS. This inertia tensor is transformed from the BDCS to the OCS using Eq. (21).

When this procedure is accomplished for all four booms, the masses, CMs, and inertia tensors in OCS will be known for all five components of the spacecraft (i.e., the central body and the four radial booms). The total spacecraft inertia tensor about the spacecraft CM is obtained by applying the parallel axis theorem again to translate the five components to the spacecraft CM,

$$J = \sum_{i=1,5} \left[J_{CM,i} + m_i (r_i^2 I_3 - \vec{r}_i \vec{r}_i^T) \right], \tag{26}$$

where here the $\vec{r}_i$ are the vectors in OCS from the spacecraft CM to the CMs of the five body components, and r_i are their magnitudes.

Note that while this paper focuses on the rigid-body inertia tensor, there also exists an "effective inertia tensor" that is used in the MMS onboard attitude maneuver controller and in the AGS Kalman filter to compute the definitive attitudes. The effective inertia is a useful concept for attitude estimation and control using rigid-body algorithms in the presence of unmodeled boom flexibility.[11,12] In the event of a boom anomaly, the techniques given here for the rigid-body inertia tensor will provide results that are needed for computing an improved effective inertia tensor as well.

SOLUTION FOR CONSISTENT SPIN AXIS AND MPA

The inner iteration algorithm described in an earlier section accepts a spin vector as a parameter and solves for the spacecraft CM and boom directions that are consistent with that spin direction. As indicated in that section, that algorithm permits the spin axis to take on values that are not consistent with torque-free steady-state motion. Recall that as the spin axis changes, the boom angles change, and consequently, the inertia tensor and MPA also change. To arrive at a full set of realistic values for the spacecraft, one must solve for the spin axis that coincides with the MPA of the resultant spacecraft geometry.

It is stressed that coincidence of the spin axis and the MPA is an assumption that is valid when all major vibrations have damped out and the system acts as five rigid bodies at equilibrium. The

actual booms are far from rigid and have many modes of vibration. However, as vibrations dampen, the booms appear nearly straight and at rest in the body frame. The system will behave approximately as a rigid body for very low-frequency perturbations, but not for thrusting or for debris impacts. When a true rigid body in stable torque-free rotation is perturbed, the instantaneous angular velocity vector will nutate about the MPA (as observed from a body-fixed coordinate system). In a flexible spacecraft, a disturbance usually will induce vibrations and internal motions that dissipate energy. After some time, the vibrational modes will fully dampen. The final equilibrium state is that at which the angle between the MPA and the instantaneous angular velocity is zero.

Outer Iteration Algorithm

The outer iteration algorithm requires only the nominal spacecraft geometry, the four boom fractions, and the remaining fraction of fuel as input to arrive at a solution for the spacecraft CM and inertia tensor. On each iteration, the CM and boom directions are recalculated because the spin axis parameter is varied. That is, each outer iteration requires full evaluation and convergence of the inner iteration algorithm described in the section on the Solution for Consistent Spacecraft CM and Boom Vectors.
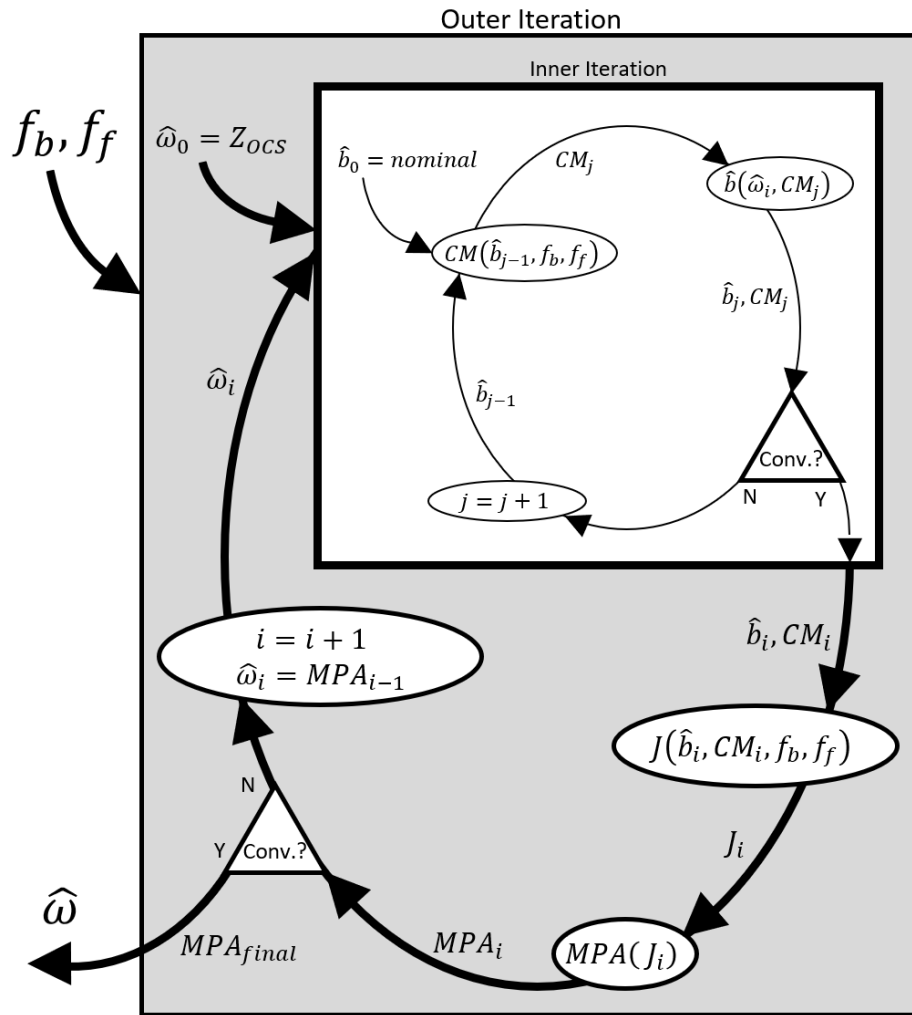

Figure 5. Functional Flow Diagram for Nested Iteration.

Figure 5 illustrates the overall process of solving for the mass properties given the boom fractions, f_b, and fuel tank fill-fraction, f_f. Note that in the figure, f_b represents the 4-tuple of the four boom fractions.

To begin the iterative process, the initial guess for the spin axis is Z_{OCS} since this is the nominal spin direction. For subsequent iterations, the MPA from the previous iteration is used as the spin axis because the hypothesis is that these vectors are coincident. For the inner iterative process, the initial guess uses the four nominal boom directions. These are the directions radial to the nominal spin axis, which extend through the boom attachment points; pictorially, the booms nominally point straight out as spokes on a wheel.

Each loop of the outer iteration models the inertia tensor using the spin axis for that iteration. This involves running the inner iteration algorithm outlined in the earlier section until it converges to obtain the CM and boom vectors that are consistent with each other and the given spin axis. The geometry dictated by the boom vectors allows calculation of the inertia tensor as described in the Inertia Tensor section. The MPA of the inertia tensor is the eigenvector of this matrix having the largest eigenvalue. If the angular difference between this MPA and the spin axis is below some threshold, the algorithm has converged; if not, the iteration continues.

Accelerated Series Convergence

When the straightforward iteration method described above is used to determine a consistent spin axis direction and MPA for the MMS spacecraft, it typically requires more than 100 iterations to converge to milli-arcsecond precision for the direction of the MPA. Inspection of the direction of the spin axis at each step of the process shows that the error decreases with each iteration and does not alternate signs. If the error decreases roughly as a power law, then it should be possible to accelerate the convergence.

Let $\hat{\omega}_i$ be the ith iteration for the MPA direction. The z-component of $\hat{\omega}_i$ will always be near unity since the MPA is near the OCS Z-axis. Let x_i and y_i be the x- and y-components of $\hat{\omega}_i$ in the OCS frame. Define the difference in the x-component at each iteration to be

$$e_i \equiv x_i - x_{i-1} .$$ (27)

The partial sum for the x-component then is

$$x_N = x_0 + \sum_{i=1}^{N} e_i .$$ (28)

Here, and in the following, the expressions for y_i are identical to those for x_i. Assume the difference term has the form of a power law; that is,

$$e_i = c\alpha^i .$$ (29)

From Eq. (29), one has

$$\alpha = \frac{e_{i+1}}{e_i} ,$$ (30)

for any i. The limit of the partial sums in Eq. (28) is

$$x_\infty = x_0 + \sum_{i=1}^{\infty} e_i = x_0 + c \sum_{i=1}^{\infty} \alpha^i = x_0 + \frac{c\alpha}{1-\alpha} ,$$ (31)

where the last summation assumes α has magnitude less than unity. Using $c\alpha = e_1$ from Eq. (29), one can rearrange Eq. (31) to find

$$x_\infty = \frac{x_1 - \alpha x_0}{1-\alpha} .$$ (32)

One can then show by induction that

$$x_\infty = \frac{x_{i+1} - \alpha x_i}{1 - \alpha},$$ (33)

for any i.
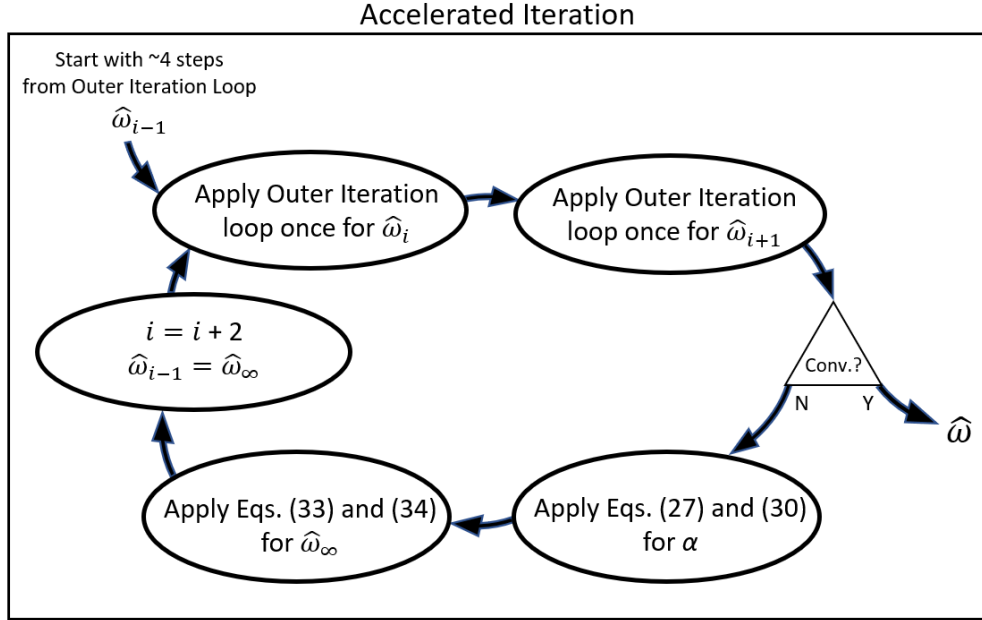
Accelerated Iteration

Figure 6. Functional Flow Diagram for Accelerated Iteration Method.

Figure 6 shows how Eqs. (27-34) can be applied to accelerate the convergence. One starts with Z_{OCS} as an initial guess for the spin axis and takes a few normal iteration steps to get the process started, as presented in Figure 5. Next, one uses the last value, $\hat{\omega}_{i-1}$, and takes two additional normal iteration steps, yielding $\hat{\omega}_i$ and $\hat{\omega}_{i+1}$. If convergence has not yet occurred, one computes e_i and e_{i+1} as in Eq. (27), solves for α using Eq. (30), and then applies Eq. (33) to obtain a new value for the x-component of the spin axis. The same steps are followed to find the y-component. One obtains the z-component from the unit norm of the vector, $z_\infty = [1 - x_\infty^2 - y_\infty^2]^{1/2}$. The components are combined to obtain

$$\hat{\omega}_\infty = [x_\infty, \ y_\infty, \ z_\infty]^T.$$ (34)

This new spin unit vector is used as the initial guess to restart the process. That is, begin with $\hat{\omega}_\infty$, take two normal iteration steps, check for convergence, and compute e_i and e_{i+1} from the last three values, etc. When convergence is achieved, the spin axis used to compute the CM and boom angles will agree with the MPA from the resulting inertia tensor to within the requested tolerance.

For a wide variety of severed boom combinations, this accelerated iteration method has been found to converge in one-tenth to one-third of the total number of steps as straightforward iteration, including accounting for the fact that there are two iteration steps for each accelerated step.

The method presented here is closely related to the Aitken's δ^2-process for accelerating the convergence of series.[13] Note that Aitken's method recommends rearranging the expression in Eq. (33) to improve numerical stability, but that change was not found to be needed for the present application.

14

DETERMINATION OF LOCATION WHERE BOOM IS SEVERED

One responsibility for the MMS AGS analysts is to estimate the direction of the MPA after every maneuver. When the spacecraft expends fuel, the mass distribution changes and a recalibration of the inertia tensor may be needed. A small change in the MPA direction has been seen after almost every maneuver, especially during the first two years of the MMS mission. This MPA shift is the result of an asymmetry in the fuel distribution. The asymmetry is caused primarily by changes in the shapes of the fuel tank diaphragms as they relax, plus possibly a contribution from differences in the fuel draw-down from the four separate tanks. This AGS capability to estimate the MPA can be used in the analysis of a boom break, as follows.

The star cameras on MMS allow for accurate attitude determination; using the AGS Kalman filter, the uncertainty in the estimated instantaneous direction of the angular momentum vector is approximately 0.005 deg and the spin phase uncertainty is 0.05 deg (3σ). With this knowledge, the MPA direction in the OCS frame can be determined with an uncertainty of 0.003 deg (3σ).[7]

Table 1. Tilt Angles φ_1 and φ_2 Versus Boom Fraction.

Fraction of Boom Remaining, f_b	φ_1 (deg)	φ_2 (deg)
1.00	-0.010	0.019
0.99	0.371	0.144
0.95	0.761	0.271
0.75	0.993	0.346
0.50	1.215	0.417
0.00	1.409	0.480

The expected MPA direction can be computed from the inertia tensor model for various break locations. By comparing these values against the observed MPA direction, a mapping can be made from the observation to the modeled break location. The two tilt angle parameters φ_1 and φ_2, introduced in the section discussing the Solution for Consistent Spacecraft CM and Boom Vectors, are given in Table 1 as a function of break location for a single broken boom (MMS SDP #1). Table 1 shows that the change in body tilt angle (i.e., change in MPA direction) is predominantly in the direction of the φ_1 angle. An important aspect of Table 1 is that both angles are monotonic in f_b. This is conducive to tabulation and lookup by interpolation, which is a convenient way to generate these results.
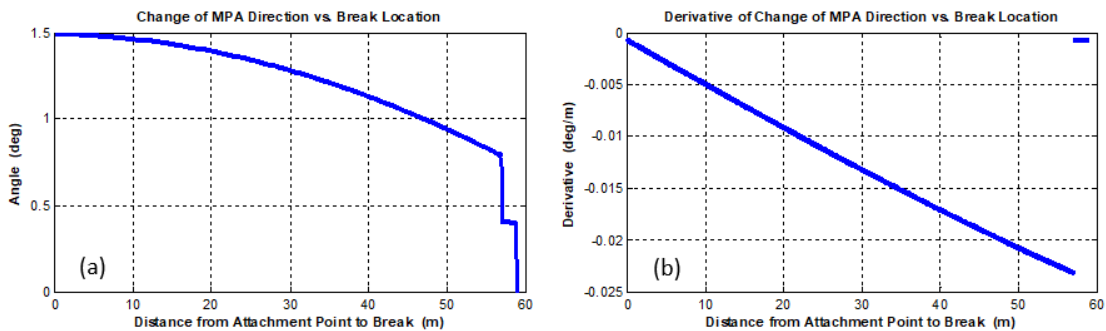

Figure 7. (a) Change of MPA direction, and (b) derivative of the change of MPA direction versus location where the boom was severed.

Since the angles shown in Table 1 are monotonic, one can define a single net angular change of MPA direction resulting from the break, reducing the interpolation to a single independent variable. Figure 7a shows the dependence of this change in the direction of the MPA on the location where the boom is severed (given here in meters rather than boom fraction). By recalibrating the MPA after such an event, the MMS analysts will be able to determine the actual change in MPA direction and then read the location of the break in the boom from this plot. In practice, Figure 7a or an equivalent table would be recalculated at the time when a break occurs to account for which boom was severed and for the current value of the fuel tank fill-fraction (a fill-fraction of 0.3 has been assumed in all the examples shown in this paper).

An error bound can be placed on the break location estimate. The uncertainty in where the boom was severed is related to the derivative of the curve in Figure 7a. Figure 7b shows this derivative, with the near-discontinuities at the locations of the preamplifier and the sensor sphere removed. Let Φ be the angular change in the MPA direction shown in Figure 7a, determined using the inertia tensor calibration procedure at the time when a break occurs.[5] Let $\Delta\Phi$ be the uncertainty in this value, taken to be 0.006 deg (twice the MPA error since this is a difference of MPAs). Denote the location of the break as X, measured from the boom attachment point. The uncertainty in X, corresponding to a given value of Φ, is

$$\Delta X \approx \left| \frac{d\Phi}{dX} \right|^{-1} \Delta\Phi \ . \tag{35}$$

This expression yields 3σ uncertainties in the estimate of the break location of 6 m for a break near the boom attachment point, approximately 50 cm for a break near the midpoint, and 20-30 cm near the boom tip.

CONCLUSIONS

The effects of a radial boom break on the spacecraft inertia tensor were shown to be observable and quantifiable. Further, it was shown that for a single broken boom, a mapping exists between the change in spacecraft MPA resulting from the break and the location of that break along the boom. This mapping can be tabulated for quick lookup and interpolation. Using only computations of the MPA direction from before and after a suspected break, an informed estimation of the break location and its uncertainty can be produced.

While examples were presented only for a single severed boom, the models and techniques developed here are also valid when the booms are whole or when there are multiple severed booms. The models consider the remaining boom fraction independently for each boom, and the current software implementation supports this feature. One possible enhancement might be to expand the technique described in the previous section to map the observed MPA direction to two boom fraction values instead of one.

The technique for determining the inertia tensor for a severed boom applies with very little modification to a boom that has not been severed but instead has failed to deploy fully. In this scenario, it would be necessary to add the mass of any undeployed wire to the central spacecraft body mass. The position of this mass would be at the location of the spool holding the wire. Also, the values given in Figures 3a and 3b would need to be modified to reflect the mass and CM for the partially deployed boom, rather than for a severed boom.

Work is underway to integrate the prototype code for the new CM and inertia tensor models into the operational AGS for the MMS mission. These improvements will provide benefits for the AGS products needed for attitude prediction, definitive attitude estimation, and onboard maneuver control. Other future work is planned to investigate how best to incorporate the new models into

the AGS calibration utility that estimates corrections to the MPA direction. When this work is complete, the AGS will have the capability to support the MMS mission immediately in case a boom is severed. Routine data products will account for the boom damage, and the software will offer insight into the boom status.

ACKNOWLEDGMENTS

REFERENCES

[1] R. Pfaff, C. Carlson, J. Watzin, D. Everett, and T. Gruner, "An Overview of the Fast Auroral SnapshoT (FAST) Satellite," *Space Science Reviews* 98(1):1-32, Aug. 2001.

[2] J.L. Burch, "IMAGE Mission Overview," *Space Science Reviews, IMAGE special issue*, 91, 1-14, Jan. 2000; see also NASA IMAGE Science Center web page, https://image.gsfc.nasa.gov/rpi/rpi_anomalies.html.

[3] D. Cosgrove, S. Frey, J. Marchese, B. Owens, and M. Bester, "ARTEMIS Operations from Earth-Moon Libration Orbits to Stable Lunar Orbits," *SpaceOps Conference*, Stockholm, Sweden, 2012.

[4] G.G. Herzl, et al., "Tubular Spacecraft Booms (Extendible, Reel Stored)," published by JPL for NASA, *NASA Space Vehicle Design Criteria (Guidance and Control)*, NASA SP-8065, Feb. 1971.

[5] J.E. Sedlak, E.A. Superfin, and J.C. Raymond, "Magnetospheric Multiscale (MMS) Mission Attitude Ground System Design," *22nd International Symposium on Spaceflight Dynamics*, INPE, São José dos Campos, SP, Brazil, Feb. 2011.

[6] F.L. Markley and J.E. Sedlak, "Kalman Filter for Spinning Spacecraft Attitude Estimation," *Journal of Guidance, Control, and Dynamics*, Vol. 31, No. 6, p. 1750, Nov.-Dec. 2008.

[7] J.C. Raymond, J.E. Sedlak, and B. Vint, "Attitude Ground System (AGS) for the Magnetospheric Multiscale (MMS) Mission," *25th International Symposium on Spaceflight Dynamics*, Munich, Germany, Oct. 2015.

[8] A.S. Sharma and S.A. Curtis, "Magnetospheric Multiscale Mission", *Nonequilibrium Phenomena in Plasmas*, Astrophysics and Space Science Library, Vol. 321, Springer-Netherlands, pp. 179–195, 2005.

[9] P.-A. Lindqvist, et al., "The Spin-Plane Double Probe Electric Field Instrument for MMS," *Space Sci. Rev.* (2016) 199:137-165, DOI 10.1007/s11214-014-0116-9.

[10] O. Hsu and J. Mccarthy, "Magnetospheric Multiscale (MMS) Project Alignment and Coordinate System Document," NASA/GSFC, 461-SYS-SPEC-0115, Rev. C, 2014.

[11] S. Mariconti, "Magnetospheric Multiscale (MMS) Project Mass Properties Report," NASA/GSFC, 461-MECH-RPT-0086, 2013.

[12] D. Zimbelman and M. Walker, "Fast Auroral Snapshot Performance Using a Multi-Body Dynamic Simulation," AAS 93-334, *AAS/NASA International Symposium on Spaceflight Dynamics*, Greenbelt, MD, April 1993.

[13] W.H. Press, B.P. Flannery, S.A. Teukolsky, and W.T. Vetterling, *Numerical Recipes, The Art of Scientific Computing*, Ch. 5, Cambridge University Press, Cambridge, 1986, ISBN 0-521-30811-9.